RSC Advances

ROYAL SOCIETY OF CHEMISTRY

www.rsc.org/advances

RSC Advances

ARTICLE

Room temperature triethylamine sensing properties of polyaniline-WO_3 nanocomposites with p-n heterojunction

Cite this: RSC Adv., 201x

Shouli Bai, Yaqiang Ma, Ruixian Luo, Aifan Chen*, Dianqing Li*

Received 00th January 20xx,
Accepted 00th January 20xx

DOI: 10.1039/x0xx00000x

www.rsc.org/

Abstract

Polyaniline (PANI)–tungsten oxide (WO_3) nanocomposites have been successfully synthesized using different weight percentages of tungsten oxide (10–50%) dispersed in polyaniline matrix by a facile in-situ chemical oxidation polymerization. The sensors based on PANI-WO_3 nanocomposites were fabricated on a substrate of polyethylene terephthalate (PET) films for detection of triethylamine (TEA) gas at room temperature. It was observed that the sensors of PANI-WO_3 nanocomposites show better sensitivity, selectivity, and reproducibility compared to pure PANI, particularly the sensor based on PANI-30% WO_3 operating at room temperature exhibits maximum response of 81 to 100 ppm TEA gas, that is 13 times higher than that of pure PANI. The sensing mechanism of the nanocomposites in presence of TEA atmosphere was discussed in detail, which is attributed to the increase of percentage of doping protonic acid and the formation of p–n heterojunction between p-type PANI and n-type WO_3.

1 Introduction

Triethylamine (TEA) is a kind of volatile organic compounds (VOCs), which has been widely used as organic solvent and catalyst in the industrial production.[1, 2] It is also released gas during the decay of fishes and seashells after death.[3, 4] It can cause great damage on human health like headaches, skin burns, nausea, eye irritation and especially respiratory difficulty due to strong pungency with result of pulmonary edema and even death. The permissible exposure limit of TEA that recommended in the workplace is 10 ppm by National Institute for Occupational Safety and Health (NIOSH).[5] Although some traditional methods like gas detection tube, gas/liquid chromatography, electrochemistry analysis, and colorimetric method are powerful for TEA detection, the complex detection process and expensive equipment hinder their wide applications.[6, 7] Thus accurate and fast detection of TEA especially for the sensor with high sensitivity is always in great demand in biomedical, chemical and food industries.

Tungsten oxide (WO_3) is well-known as a n-type semiconductor sensing material with a band-gap of 2.6–3.0 eV,[8] and has sensing response to some of toxic gases due to its non-stoichiometry.[9, 10] But the application of pure WO_3 sensing material is limited by its high operating temperature, high power consumption, safety hazards and low selectivity. Compared with traditional inorganic semiconductor oxide materials, conducting polymers such as polyaniline (PANI), polypyrrole (PPy) and polythiopene (PTh), have attracted increasing attentions over the past decade. The most attractive character of conducting polymer gas sensor is that the response to a wide range of VOCs at ambient temperature. Among various conducting polymers, polyaniline (PANI) is of great interest because PANI shows diverse chemical structures and various response mechanisms upon exposure to different gases.[11-14] However, these conducting polymers usually show a poor thermal, mechanical, oxidative stability and low sensitivity to detect gas that limits their potential applications in future.[15-17] In order to overcome these problems, several improved methods have been studied. For example, by morphological design of PANI, doping of noble metals , and incorporating inorganic metal oxide or carbon based materials to enhance the sensitivity of PANI for specific applications in the sensors.[18] Patil et al.[19] prepared room-temperature ammonia sensors based on copper nanoparticle intercalated polyaniline nanocomposite thin film, and the sensor

State Key Laboratory of Chemical Resource Engineering, Beijing Key Laboratory of Environmentally Harmful Chemicals Analysis, Beijing University of Chemical Technology, Beijing 100029, China

containing 0.13 at.% of Cu showed the response of 1.86 to 50 ppm NH_3. Bandgar et al.[20] designed a polyaniline/iron-oxide (PAni/α-Fe_2O_3) nanocomposite based ammonia sensor and the response of the sensor is 1.39 when exposed to 100 ppm NH_3 gas. Mitesh et al.[21] synthesized graphene/PANI nanocomposite with the response of 1.12 to 100 ppm toluene at 50 °C. Up to now, there are less reports relatively about TEA gas sensors operated at room temperature. In order to lower the operating temperature and improve the sensitivity of TEA gas sensors, hybridization of the polyaniline and inorganic WO_3 nanoparticles will produce new sensing materials, and their sensing performance will exceed the constituent counterparts due to the synergistic effect between the polyaniline and metal oxide.[15, 22, 23]

In the present work, we have prepared a series of PANI-WO_3 nanocomposites and loaded on flexible polyethylene terephthalate (PET) films to fabricate the smart sensors for detection of different concentrations of TEA at room temperature (25 °C). The sensing mechanism of the material to TEA and the key factor enhanced gas sensing were discussed by XPS. The work may open the window for PANI/metal oxide composites in applications of the area of micro/nano-electronic devices.

2 Experimental details

2.1 Preparation of WO_3 nanoparticles

WO_3 nanoparticles were synthesized by a colloidal chemical method based on sodium tungstate dehydrate ($Na_2WO_4{\cdot}2H_2O$, analytical grade). 1 g $Na_2WO_4{\cdot}2H_2O$ was dissolved into 60 mL deionized water. Then a certain concentration of aqueous solution of HCl was dropwise added to the sodium tungstate solution under stirring at room temperature till no white precipitate was further formed. Then the solution was aged for 24 h, after which a quantity of cetyltrimethyl ammonium bromide (CTAB) solution (15 ml, 0.15 mol/L) was immediately added to the solution and abundant white flocculent precipitate was formed. The white flocculent precipitate was treated by ultrasonication for 40 min and after that the precipitate was filtrated and centrifuged with deionized water and ethanol to remove Cl^-, Br^- and any other possible remnants. At last the precipitate was dried at 50 °C and calcined at 600 °C for 2 h to obtain the WO_3 nanoparticles.

2.2 Synthesis of PANI-WO_3 nanocomposites

The PET (1cm×1cm) films as the sensor substrates were pretreated in a 0.02 g/mL NaOH solution at 95 °C for 90 min and dried with ethanol at 50 °C. Aniline hydrochloride, ammonium peroxydisulfate (APS), hydrochloric acid and N-methyl-2-pyrrolidone (NMP) were all of analytical grade and were used without further purification. The PANI-WO_3 nanocomposites were synthesized by a facile in-situ chemical oxidation polymerization of aniline with APS as the oxidant in the presence of WO_3 nanoparticles. In a typical synthetic procedure, 1.5mmol aniline monomer and different weight percentage of WO_3 powder (e.g. 0%, 10%, 20%, 30%, 40 % and 50%) were separately dissolved in 15mL 1M hydrochloric acid solution. Then the solution was dealt with ultrasonication for 15 min. Another 15mL 1M hydrochloric acid solution containing the same mol APS which was cooled in ice cold solution in advance was immediately added to the above solution with continuous stirring at 0-5 °C for 30 min. The products were filtered and washed with deionized water, ethanol and 1 M HCl sequentially. Finally, the precipitates were dried in air at 50 °C and a series of PANI-WO_3 nanocomposites were prepared. Appropriate amount of the above obtained PANI-WO_3 powders with some amount of NMP (N-methylpyrrolidone) were mixed and grinded adequately in an agate morto to gain a uniform mixture. The obtained mixtures were smeared on the surface of PET films and denoted as PANI, PW10, PW20, PW30, PW40 and PW50 with respect to the corresponding WO_3 weight percentages of PANI. Fig. 1 shows the schematic illustration of the fabrication of the gas sensor based on PANI-WO_3 nanocomposites.

2.3 Characterization of the samples

The characterization analysis of PANI-WO_3 samples were carried out using XRD, FTIR, Raman, FESEM, UV-Vis, TG and XPS techniques. For crystal structure analysis, Powder X-ray diffraction (XRD) patterns of the products were recorded on a Rigaku D/MAX-2500 X-ray diffractometer at 30 kV and 100 mA with copper Kα radiation (λ= 1.54Å). Scanning rate of 5° min^{-1} was applied to record the patterns in range of 10–70° (2θ). Fourier transform infrared (FT-IR) spectra were recorded on a FT-IR absorption spectrometer (Nicolet 6700) at room temperature. The Raman spectra measurements were carried out on a Raman spectrometer (HR-800, λ_{exc} = 532 nm) at room temperature. The microscopic structure of PET samples observed by Field emission scanning electron microscopy (FESEM) images were obtained with a Hitachi S-4700 instrument operated at 20.0 kV. The UV–Vis absorption spectra of the samples in methanol solvent were recorded in the range of 200–800 nm with a Shimadzu UV-2550, UV–Vis spectrophotometer (Japan). The thermogravimetric (TG) analysis was carried out in dynamic nitrogen atmosphere (75 mL min^{-1}) with a heating rate of 10 °C min^{-1} using NETZSCH STA 449 F3 thermal analyzer. X-ray photoelectron spectra (XPS) were recorded on a VG ESCALAB-MK electron spectrometer with Al Kα as the excitation source.

2.4 Sensor fabrication and response measurement

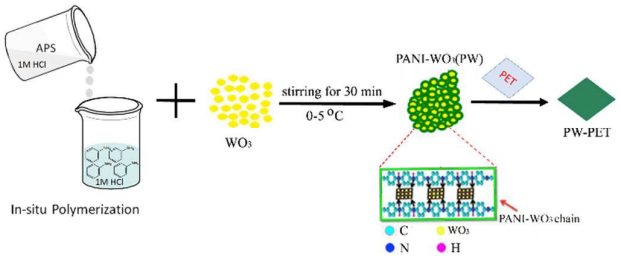

Fig.1 Schematic diagram of the fabrication process of TEA sensor based on PANI-WO_3 nanocomposites.

The chemical sensors were constructed using the PET films with PANI-WO_3 nanocomposites which were welded on a special pedestal with six poles by silver pulp. The gas sensing properties of pure PANI and PANI-WO_3 nanocomposites were measured using a JF02E gas sensor test system (Guiyang Jinfeng Technology Co., Kunming, China). The constructed sensors were installed into an 18 L air chamber. TEA was used as the test gas to test the gas performance of PANI and PANI-WO_3 nanocomposites at room temperature. Test gases with different concentrations were introduced into the air chamber via a syringe. After every test, the chamber should be opened to diffuse test gas away. The resistance of the sensor in air (R_{air}) and in the air–test gas mixture (R_{gas}) was recorded, respectively. The response for reducing gas TEA is defined as the ratio of R_{gas}/R_{air}. The response time and recovery time of the sensor were measured as the time taken for the sensor output to reach 90% of its saturation after applying or switching off the gas in a step function.

3 Results and discussion

3.1 Structure, morphology and thermal stability of PANI, WO_3 and PANI-WO_3 (PW30)

Fig. 2 depicts the X-ray diffraction pattern of the pure PANI, pure WO_3 nanoparticles and PANI-WO_3 nanocomposites. Fig. 2(a) shows the pure PANI has a broad peak at 2θ = 20°-30° without other obvious diffraction peaks.[24] Fig. 2(b) represents the X-ray diffraction pattern of WO_3, in which diffraction peaks at 2θ = 23.10°, 23.71°, 24.07°, 26.57°, 28.77°, 34.02°, 41.52°, 47.23°, 49.33° and 55.11° are assigned to the scattering from (001), (020), (200), (120), (111), (220), (221), (002) , (400) and (401) planes and well match with the JCPDS card no.20-1324.[25] Compared to pure WO_3, Fig. 2(c) and Fig. S1(a) show the X-ray diffraction pattern of the PANI-WO_3 nanocomposites, which indicates that the nanocomposites appear a small broad peak at 2θ = 20°-30°due to the addition of WO3 nanoparticles during polymerization, and also indicates the structure and property of WO_3 crystalline phase have not been changed.

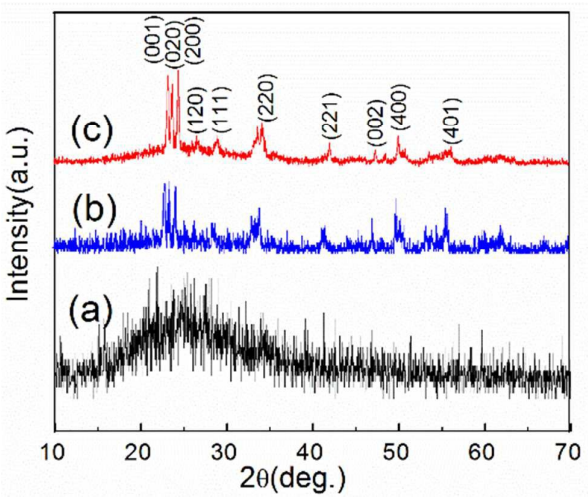

Fig.2 XRD patterns of (a) PANI, (b) WO_3 and (c) PANI-WO_3 (PW30).

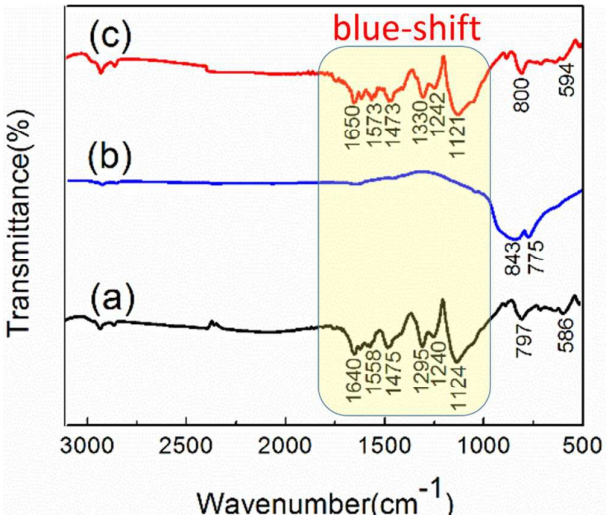

Fig.3. FT-IR spectra of (a) PANI, (b) WO_3 and (c) PANI-WO_3 (PW30).

Fourier transform infrared spectroscopy (FT-IR) as a non-destructive detection method is used to detect the adsorbed impurities in PANI, WO_3 and PANI-WO_3 nanocomposites. Fig. 3(a) and Fig. 3(c) show strong bands in the region 550–1700 cm^{-1} which are the characteristics of PANI. Fig. 3(a) shows the FT-IR spectrum of the pure PANI, which prepared by in-situ chemical oxidation polymerization contains all the characteristic peaks of PANI. The spectrum shows the vibration band of the dopant anion (HCl-PANI) (1124 cm^{-1}), C–N stretching mode in Ar-NH-Ar (1295 cm^{-1}), C=C stretching mode of benzenoid rings (1475 cm^{-1}), C=C stretching mode of the quinoid rings (1558 cm^{-1}), and the C–H bending vibration out of the plane of the paradisubstituted benzene rings (797 cm^{-1}).[26, 27] The IR spectra indicate that Fig. 3(a) is pure polyaniline. Fig. 3(b) shows the W–O bond stretching mode appears as a broad band around 843 cm^{-1}. As can be seen, the Fig. 3 (c) spectrum exhibits the main characteristic bands of PANI. Because of the IR intensity of the inorganic WO_3 is far weaker than that of the organic PANI and the relative low amount of WO_3 in nanocomposites. The blue-shift of these bands with the addition of WO_3 indicates a synthetic effect of PANI-WO_3.[28]

Raman spectroscopy was employed to study the structural characterization of the products. Fig. 4 shows a selected region of Raman spectra of the pure PANI, WO_3, as well as PANI-WO_3 (PW30). Generally, there are three regions in Raman spectrum of polyaniline that are sensitive to the level of oxidation and the protonation degree in Fig. 4(a): (1) 1167 cm^{-1}, where C–H bending vibrations of benzene or quinone type rings are most prominent; (2) 1482 cm^{-1} with characteristic C–N, C=N and C∼N^+ (where ∼ denotes an intermediate bond between a single and a double) stretching vibrations; (3) 1586 cm^{-1} with the dominating C–C and C=C stretching vibration of benzene and quinone type rings, respectively.[29, 30] As expected, Fig. 4(b) depicts the Ramanspectrum of WO_3. The intense peaks centered at 721 and 809 cm^{-1} correspond to the O-W-O stretching modes.

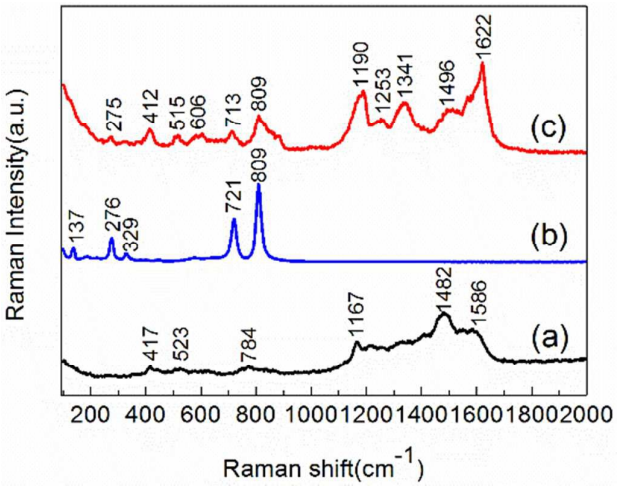

Fig.4 Raman spectra of (a) PANI, (b) WO_3 and (c) PANI-WO_3 (PW30).

The sharp peaks at 276 and 329 cm^{-1} are assigned to the O-W-O bending vibration.[31, 32] The PANI and WO_3 peaks are still observed in Fig. 4(c), indicating the presence of PANI and WO_3 in the PANI-WO_3 nanocomposites. Compared to pure PANI, the peaks at 1190, 1496 and 1622 cm^{-1} in PANI-WO_3 are broadened and move upward, probably due to the formation of C-O-W and N-O-W bonds between the PANI and WO_3 nanoparticles. These chemical bonds imply that WO_3 was chemically bonded to PANI via C-O-W and N-O-W bonds, rather than physically interacting with PANI and might be beneficial for effective charge transfer in the gas sensing measurement.

The morphology of PANI, WO_3, PW10 and PW30 are investigated by field emission scanning electron microscopy (FESEM) and typical results are shown in Fig. 5 and Fig.S2. It is found that the pure PANI exhibits some nanofibers and agglomerations. Most WO_3 nanoparticles are uniform with the diameter of 200 nm approximately and a few agglomerations. Fig. 5(c), Fig. 5(d) and Fig.S3 are PANI-WO_3

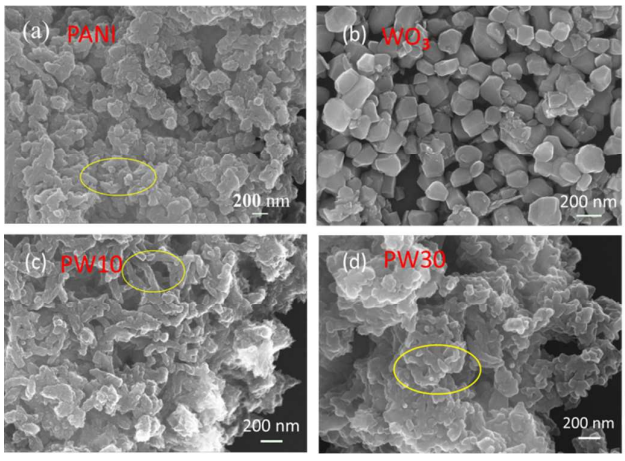

Fig.5 FESEM images of (a) PANI, (b) WO_3, (c) PW10 and (d) PW30.

nanocomposites. The PANI was wrapped on the WO_3 nanoparticles by an in-situ chemical oxidation polymerization to obtain the composite. When WO_3 nanoparticles immersed into the aniline monomer solution, free aniline or anilinium ion in the bath may adsorb preferably at the surface of WO_3 nanoparticles for the H atoms of $–NH_2–$ groups undergoing some degree of hydrogen bonding with surface O atoms or hydroxyls of WO_3 nanoparticles. Lots of WO_3 nanoparticles are coated on the surface of PANI and enwrapped by PANI, which is contributed to the formation of PANI-WO_3 nanocomposites.

The UV-Visible absorption spectra corresponding to pure PANI, WO_3 and PANI-WO_3 (PW30) powder samples dissolved in ethanol are shown in Fig. 6(1). The absorption peaks of PANI powder were recorded at 243 nm and 473 nm in Fig. 6(1a). The absorption band in the UV region is attributed to the chain of the aromatic nuclei and corresponds to the π–π* transitions and the absorption band appearing in the visible region, attributed to an interaction between the benzenic nuclei and the quinone di-imine structure.[17] Fig. 6(1b) had shown an absorption band characteristic of WO_3 at wavelength 243 nm. Fig. 6(1c) showed the PANI-WO_3 nanocomposites have two absorption peaks at 320 nm and 471 nm. Compared with the pure PANI and WO_3, the typical diversification of PANI-WO_3 is the peak at 243 nm brought about obvious red-shift, which was ascribed to the state-change of polarons from localization to delocalization, suggesting that the conformation of PANI molecular chains changed from compact to extend. Thermal gravimetric analysis curves of PAN and PANI-WO_3 are depicted in Fig. 6(2) and Fig. S1(b). Pristine PANI exhibits a three-step mass loss, pure WO_3 almost no mass loss while PANI-WO_3 nanocomposites also show homologous three-step mass loss profiles.[33] The first mass loss occurring below 155 °C for PANI and 162 °C for PANI-WO_3 are the elimination of absorbed moisture. The second mass loss occurring in 155-476 °C for PANI and 162-492 °C for PANI-WO_3 are due to the thermal elimination of dopant species and low molecular mass polymer fragments. The third mass loss in 476-701 °C for PANI and 492-709 °C for PANI-WO_3 are attributed to the degradation of the skeletal polyaniline chain structures.[27] Compared the decomposition temperature in three mass loss process, it can be seen that the thermal stability of composites is enhanced.

Surface sensitive X-ray photoelectron spectra (XPS) provide further evidence for the stronger interactions existing in PANI-WO_3 nanocomposites. The W 4f core-level spectra of WO_3 and PANI-WO_3 nanocomposites are shown in Fig. 7(a) and (b). Both of them can be decomposed into two components (W^{6+} and W^{5+}). The peak positions corresponding to W^{6+} state occur at 35.1 and 37.2 eV, while for the W^{5+} state these occur at 34.6 and 36.4 eV.[34] Compared with the pure WO_3, the four peaks of PANI-WO_3 nanocomposites moved to higher binding energy levels and all of them increased 0.5-0.6 eV. The peak shift could be ascribed to the charge transfer between PANI molecular

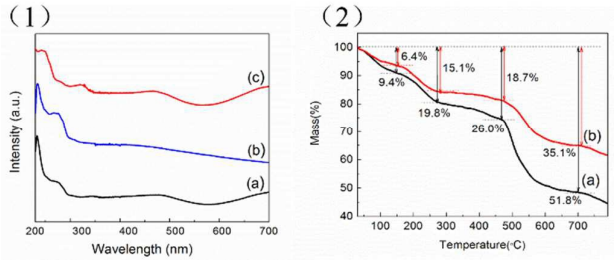

Fig.6 (1) UV-Vis absorption spectra of (a) PANI, (b) WO3 and (c) PANI-WO_3 (PW30) and (2) TGA curve of (a) PANI and (b) PANI-WO_3 (PW30).

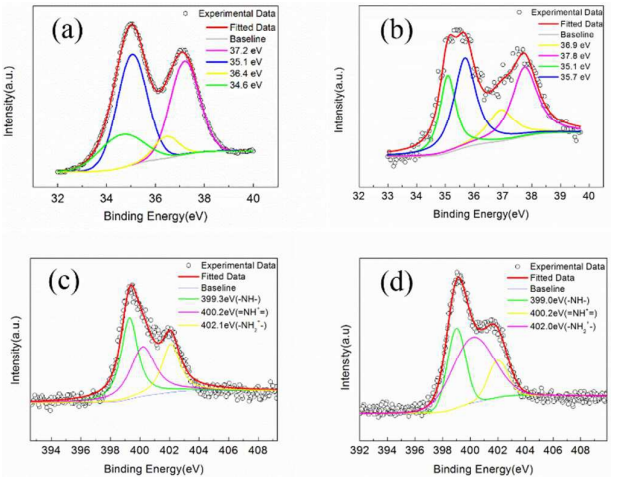

Fig.7 W 4f XPS peaks of (a) WO_3 and (b) PANI-WO_3 (PW30) and N 1s XPS peaks of (c) PANI and (d) PANI-WO_3 (PW30).

chains and WO_3 through the strong p-n heterojunction interaction. Actually, the molecular formula of the WO_3 could be written as WO_{3-x}, where x represents the number of oxygen vacancies. By calculating the area ratio of W^{6+} to W^{5+} from XPS spectrum, the x can be confirmed 0.11 for the pure WO_3 and 0.18 for the WO_3 of PANI-WO_3 nanocomposites, which indicated the molecular formula of the pure WO_3 should be written as $WO_{2.89}$ and $WO_{2.82}$ of PANI-WO_3 nanocomposites. The improvement of the non-stoichiometric feature of PANI-WO_3 nanocomposites implies their potential gas-sensing applications.[35] Fig. 7(c) shows N 1s XPS peaks of the pure PANI, which are decomposed into imine nitrogen (–NH-) with a binding energy of 399.3 eV, amine nitrogen (=NH^+=) with a binding energy of 400.2 eV and positively charged nitrogen (-NH_2^+-) with a binding energy of 402.1 eV, respectively.[36] The percentage of total areas from protonated nitrogen atoms is 60.64%, and the percentage of total protonic acid areas of PANI-WO_3 is 70.51% which significantly higher than that of pure PANI. Thus the addition of WO_3 in the polymerization process improved the percentage of total protonic acid areas and may contribute to improve the gas sensing properties.

3.2 Gas-sensing properties of PANI and PANI-WO_3 hybrids

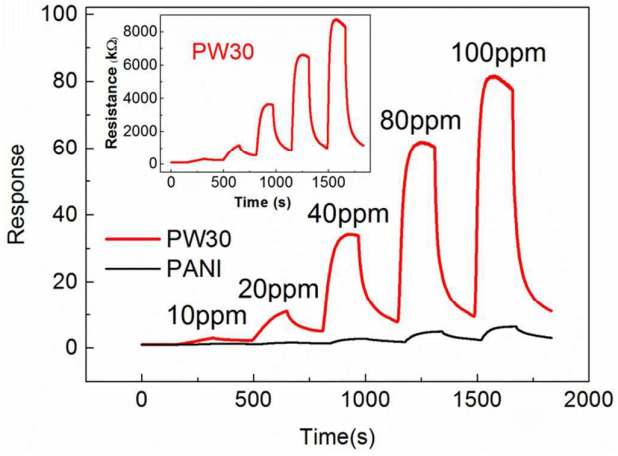

Fig.8 Responses and the transient resistances of sensors based on PANI and PANI-WO_3 (PW30) to 10-100 ppm TEA at room temperature.

Fig. 8 shows the responses of the sensors based on the pure PANI and PANI-WO_3 nanocomposites and transient resistances of sensors based on PW30 to TEA examined at room temperature (25 °C) and relative humidity of 40±1%RH. Transient resistances of sensors based on PANI and PANI-WO_3 (PW30) were shown in Fig. 8 and Fig.S3. The response of the PW30 to 100 ppm TEA reached 81, which is 13 times than that of pure PANI, and the latter only reached 6.3. Obviously, compared with pure PANI, the response of PANI-WO_3 sensor has been significantly improved. The response and recovery times are also important parameters for gas sensors, and these were defined as the time to reach 90% of the final equilibrium value after the detected gas was injected and removed, respectively. With the increase of TEA concentration, the response time and recovery time decrease. A comparison of the sensing performances between the sensor fabricated in this work and literature reports is summarized in Table 1. From the table, it can be observed correspondingly high gas response and low working temperature. In conclusion, the high gas sensitivity and the fast response-recovery time at room temperature all suggest that PANI-WO_3 nanocomposites can be an ideal candidate for TEA detecting at room temperature.

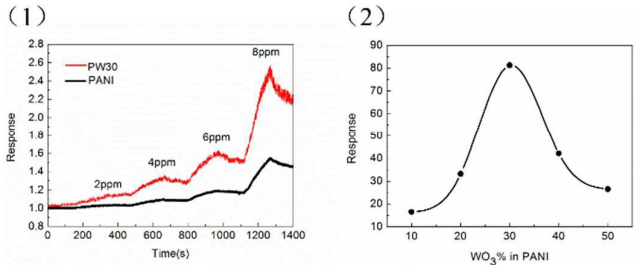

Fig.9 (1) Responses of sensors of PANI and PANI-WO_3 (PW30) to 2-8 ppm TEA at room temperature and (2) Plot of responses of PANI-WO_3 nanocomposites with different wt% of WO_3 to 100 ppm TEA at room temperature.

Table 1 Gas responses to TEA in the present study and those reported in the literatures.

Sensor material	TEA (ppm)	Operating temperature	Response	Reference
hexagonal brick-shaped SnO_2	100	160 °C	70	37
NiO/SnO_2 hollow spheres	100	220 °C	267.5	38
Ag/Cr_2O_3 microspheres	50	92 °C	52.9	39
TiO_2 nanorod arrays	100	290 °C	14.2	40
Flower-like -MoO_3	100	250 °C	416	41
polyaniline-polypyrrole coaxial nanofibers	100	Room temperature	1.5	42
PANI-WO_3 nanocomposites	100	Room temperature	81	Present study

The responses of sensors of PANI and PANI-WO_3 (PW30) to low concentration TEA were also detected at room temperature as shown in Fig. 9(1). The sensor based on PANI-WO_3 (PW30) still exhibits excellent gas sensing performance in lower TEA gas concentration with respect to pure PANI. The detection limit (D_L), defined as the lower concentration in which the response is 3 times the standard deviation of noise (instrumental detection limit).[43] Thus the D_L of PW30 is between 4 ppm and 2 ppm and lower than that of the pure PANI, which indicated PANI-WO_3 nanocomposites have high potential applications in detecting lower TEA level. Fig. 9(2) describes the plot of responses of PANI-WO_3 with different wt% of WO_3 to 100 ppm TEA at t room temperature (25 °C). It can be observed that the response of sensors based on PANI-WO_3 nanocomposites increased with the increase in the weight percentage of WO_3 and optimized for PANI-WO_3 nanocomposites synthesized with the addition of 30 wt% WO_3. A significant enhancement in the response of gas sensor based on PW30 has been observed. With further increase of WO_3 powder during synthesis process the sensor response decreased. The reason for the variation in the sensor response is due to varied morphology. With the addition of WO_3, the surface area will decreased owing to the agglomeration.

It should be noted that selectivity is an important property in a sensor system. Based on this purpose, Fig. 10 represents the sensor of PANI-WO_3 (PW30) to TEA gas for 100 ppm of

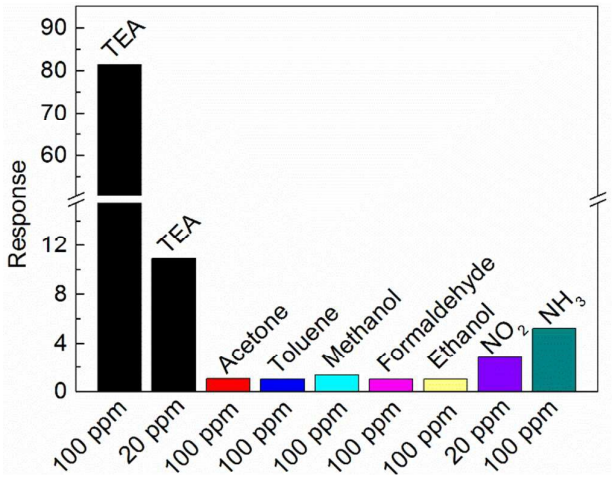

Fig.10 Response of the sensor based on PANI-WO_3 (PW30) to different tested gases at room temperature.

100 ppm of TEA, acetone, toluene, methanol, formaldehyde, ethanol, NH_3 and 20 ppm of TEA and NO_2 at room temperature. It can be obviously seen that the sensor based on the PANI-WO_3 nanocomposites has a larger response to TEA compared to the other gases. The results indicate that the sensor has a good selectivity to TEA at room temperature.

3.3 Sensing mechanism of PANI-WO_3 nanocomposites

Here, the enhancement of sensing properties to TEA could be ascribed to the increase of the percentage of doping protonic acid, which has been confirmed by XPS analysis. The deprotonation-reprotonation process of PANI plays an important role in the enhancement of the sensing performance after exposure of the sensor to TEA. PANI is protonated by the doping protonic acid during the polymerization process. When TEA is injected into test chamber, PANI in the form of emeraldine salt was reduced to emeraldine base.[44] Therefore, the holes (polaron and bipolaron sites in PANI) density in the PANI is lowered, resulting in the increase of resistance. Thus the increase of the percentage of doping protonic acid contributes to the improvement of gas sensing properties. Meantime, the experimental results obviously suggested that the nanocomposites exhibit p-type semiconductor sensing properties due to resistance increase in TEA, which should be correlated with a p–n heterojunction formed at the interface between p-type PANI and n-type WO_3. As we all know, WO_3 shows n-type conductivity by electrons, therefore it is inferable that electron mainly flow occurs from n-WO_3 to p-PANI until establishment of equilibrium and make the Fermi level (E_F) equal in n and p regions. The mutual interaction thus produces the p-n heterojunction, as shown in Fig. 11(a).[33] Fig. 11(b) and (c) show the sensing mechanism model at room temperature for the sensor based on p-type release electrons to combine with holes in p-type PANI,

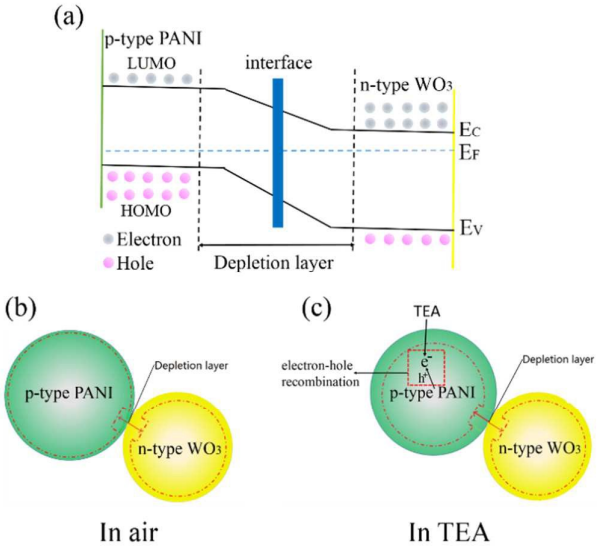

Fig.11 (1) (a) The energy band structure diagram of p-type PANI-n-type WO_3 heterojunction. (b) and (c) Schematic model for the p-type PANI-n-type WO_3 heterojunction based sensors when exposed to air and TEA gas.

leading to a decreased holes concentration. Meanwhile the electron transfer between n-WO_3 and p-PANI is hindered because of the potential barrier in the internal field. Thus, the depletion layer becomes thicker than that of it in air. This further increase the resistance of the sensor based on PANI-WO_3 nanocomposites.[38, 45] In short, the response to TEA is greatly improved due to the formation of p–n heterojunction. The resistance of PANI-WO_3 nanocomposites changes so dramatically that it is easy to detect TEA with high sensitivity at room temperature.

4 Conclusions

In summary, WO_3 nanoparticles were prepared by a facile colloidal chemical method and combined with PANI to form PANI-WO_3 nanocomposites by an in-situ chemical oxidation polymerization. Then the nanocomposites loaded on the PET film to structure a smart sensor. The response of the sensor based on PANI-30%WO_3 nanocomposites to 100 ppm TEA is 81 at room temperature (25 ^{o}C), which is 13 times higher than that of pure PANI and much higher than that of reported other sensing materials to TEA at room temperature. The sensor not only exhibits high sensitivity but also has excellent selectivity to acetone, toluene, methanol, formaldehyde and ethanol, and has flexible, inexpensive and portable characters. The mechanism enhanced PANI to TEA sensing properties could be attributed to the increase of the percentage of protonic acid and the formation of p–n heterojunction between PANI and WO_3. Therefore, it is expected that the PET conducting films with PANI-WO_3 nanocomposites can be potentially used as promising gas sensors for detecting TEA at room temperature.

Acknowledgements

This work was supported by the National Natural Science Foundation of China (Grant No. 21177007 and 51372013), the Fundamental Research Funds for the Central Universities (YS1406) and Beijing Key Laboratory of Environmentally Harmful Chemicals Analysis.

† Electronic Supplementary Information (ESI) available: supporting figures. See DOI: 10.1039/c000000x/

Notes and references

1. M. Bietti and M. Salamone, *Org. Lett.*, 2010, **12**, 3654-3657.
2. L. Xu, H. Song, J. Hu, Y. Lv and K. Xu, *Sens. Actuators B*, 2012, **169**, 261-266.
3. W.-H. Zhang and W.-D. Zhang, *Sens. Actuators B*, 2008, **134**, 403-408.
4. M. Wu, X. Zhang, S. Gao, X. Cheng, Z. Rong, Y. Xu, H. Zhao and L. Huo, *CrystEngComm*, 2013, **15**, 10123-10131.
5. Y. Xie, J. Du, R. Zhao, H. Wang and H. Yao, *Journal of Environmental Chemical Engineering*, 2013, **1**, 1380-1384.
6. E. Filippo, D. Manno, A. Buccolieri and A. Serra, *Sens. Actuators B*, 2013, **178**, 1-9.
7. H. Nohta, H. Satozono, K. Koiso, H. Yoshida, J. Ishida and M. Yamaguchi, *Anal. Chem.*, 2000, **72**, 4199-4204.
8. F. Wang, C. Di Valentin and G. Pacchioni, *ChemCatChem*, 2012, **4**, 476-478.
9. B. Xiao, Q. Zhao, C. Xiao, T. Yang, P. Wang, F. Wang, X. Chen and M. Zhang, *CrystEngComm*, 2015, **17**, 5710-5716.
10. A. Maity and S. B. Majumder, *Sens. Actuators B*, 2015, **206**, 423-429.
11. G. D. Khuspe, D. K. Bandgar, S. Sen and V. B. Patil, *Synth. Met.*, 2012, **162**, 1822-1827.
12. K. Wetchakun, T. Samerjai, N. Tamaekong, C. Liewhiran, C. Siriwong, V. Kruefu, A. Wisitsoraat, A. Tuantranont and S. Phanichphant, *Sens. Actuators B*, 2011, **160**, 580-591.
13. S. T. Navale, A. T. Mane, G. D. Khuspe, M. A. Chougule and V. B. Patil, *Synth. Met.*, 2014, **195**, 228-233.
14. A. Joshi, S. A. Gangal, N. Padma, D. K. Aswal and S. K. Gupta, *BARC Newsl.*, 2008, **297**, 236-239.
15. J. Huang, T. Yang, Y. Kang, Y. Wang and S. Wang, *J. Nat. Gas Chem.*, 2011, **20**, 515-519.

16. M. Xu, J. Zhang, S. Wang, X. Guo, H. Xia, Y. Wang, S. Zhang, W. Huang and S. Wu, *Sens. Actuators, B*, 2010, **146**, 8-13.
17. V. Talwar, O. Singh and R. C. Singh, *Sens. Actuators B*, 2014, **191**, 276-282.
18. A. Z. Sadek, W. Wlodarski, K. Shin, R. B. Kaner and K. Kalantar-zadeh, *Synth. Met.*, 2008, **158**, 29-32.
19. U. V. Patil, N. S. Ramgir, N. Karmakar, A. Bhogale, A. K. Debnath, D. K. Aswal, S. K. Gupta and D. C. Kothari, *Appl. Surf. Sci.*, 2015, **339**, 69-74.
20. D. K. Bandgar, S. T. Navale, M. Naushad, R. S. Mane, F. J. Stadler and V. B. Patil, *RSC Adv.*, 2015, **5**, 68964-68971.
21. M. Parmar, C. Balamurugan and D.-W. Lee, *Sensors*, 2013, **13**, 16611-16624, 16614 pp.
22. A. Kaushik, R. Khan, V. Gupta, B. D. Malhotra, S. Ahmad and S. P. Singh, *J. Nanosci. Nanotechnol.*, 2009, **9**, 1792-1796.
23. C. A. Betty, S. Choudhury and S. Arora, *Sens. Actuators B*, 2015, **220**, 288-294.
24. G. D. Khuspe, S. T. Navale, M. A. Chougule and V. B. Patil, *Synth. Met.*, 2013, **185–186**, 1-8.
25. H. Xia, Y. Wang, F. Kong, S. Wang, B. Zhu, X. Guo, J. Zhang, Y. Wang and S. Wu, *Sens. Actuators B*, 2008, **134**, 133-139.
26. L. Geng, Y. Zhao, X. Huang, S. Wang, S. Zhang and S. Wu, *Sens. Actuators B*, 2007, **120**, 568-572.
27. A. A. Khan and M. Khalid, *J. Alloy. Compd.*, 2010, **117**, 1601-1607.
28. B.-X. Zou, X.-X. Liu, D. Diamond and K.-T. Lau, *Electrochim. Acta*, 2010, **55**, 3915-3920.
29. G. Ciric-Marjanovic, M. Trchova and J. Stejskal, *J. Raman Spectrosc.*, 2008, **39**, 1375-1387.
30. R. Mazeikiene, V. Tomkute, Z. Kuodis, G. Niaura and A. Malinauskas, *Vib. Spectrosc.*, 2007, **44**, 201-208.
31. S. Zhuiykov and E. Kats, *Ionics*, 2015, **21**, 775-784.
32. X. Chu, T. Hu, F. Gao, Y. Dong, W. Sun and L. Bai, *Mat. Sci. Eng. B-Solid.*, 2015, **193**, 97-104.
33. C. Murugan, E. Subramanian and D. P. Padiyan, *Synth. Met.*, 2014, **192**, 106-112.
34. A. P. Shpak, A. M. Korduban, M. M. Medvedskij and V. O. Kandyba, *J. Electron Spectrosc. Relat. Phenom.*, 2007, **156-158**, 172-175.
35. S. Bai, K. Zhang, L. Wang, J. Sun, R. Luo, D. Li and A. Chen, *J. Mater. Chem. A*, 2014, **2**, 7927-7934.
36. L. Wang, Q. Yao, H. Bi, F. Huang, Q. Wang and L. Chen, *J. Mater. Chem. A*, 2015, **3**, 7086-7092.
37. Y. Xie, J. Du, R. Zhao, H. Wang and H. Yao, *J. Environ. Chem. Eng.*, 2013, **1**, 1380-1384.
38. D. Ju, H. Xu, Q. Xu, H. Gong, Z. Qiu, J. Guo, J. Zhang and B. Cao, *Sens. Actuators B*, 2015, **215**, 39-44.
39. J. Cao, Y. Xu, L. Sui, X. Zhang, S. Gao, X. Cheng, H. Zhao and L. Huo, *Sens. Actuators B*, 2015, DOI: 10.1016/j.snb.2015.06.023, Ahead of Print.
40. H.-y. Yang, X.-L. Cheng, X.-F. Zhang, Z.-k. Zheng, X.-f. Tang, Y.-M. Xu, S. Gao, H. Zhao and L.-H. Huo, *Sens. Actuators B*, 2014, **205**, 322-328.
41. L.-l. Sui, Y.-M. Xu, X.-F. Zhang, X.-L. Cheng, S. Gao, H. Zhao, Z. Cai and L.-H. Huo, *Sens. Actuators B*, 2015, **208**, 406-414.
42. S. Weng, J. Zhou and Z. Lin, *Synth. Met.*, 2010, **160**, 1136-1142.
43. T. Krishnakumar, R. Jayaprakash, N. Pinna, N. Donato, A. Bonavita, G. Micali and G. Neri, *Sens. Actuators B*, 2009, **143**, 198-204.
44. Z.-F. Li, F. D. Blum, M. F. Bertino, C.-S. Kim and S. K. Pillalamarri, *Sens. Actuators B*, 2008, **134**, 31-35.
45. S. Bai, H. Liu, R. Luo, A. Chen and D. Li, *RSC Adv.*, 2014, **4**, 62862-62868.

Room temperature triethylamine sensing properties of polyaniline-WO_3 nanocomposites with p-n heterojunction

Shouli Bai, Yaqiang Ma, Ruixian Luo, Aifan Chen,*Dianqing Li*

State Key Laboratory of Chemical Resource Engineering, Beijing Key Laboratory of Environmentally Harmful Chemicals Analysis, Beijing University of Chemical Technology, Beijing 100029, China

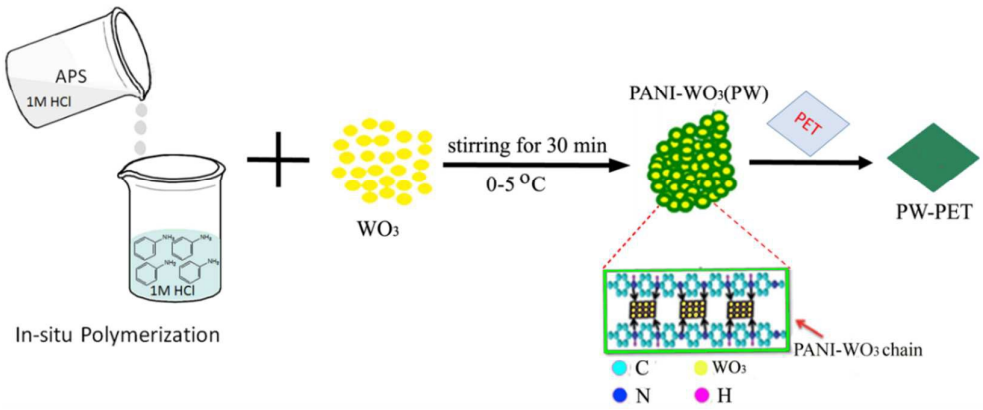

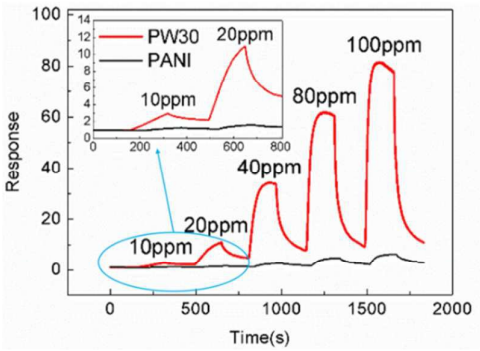

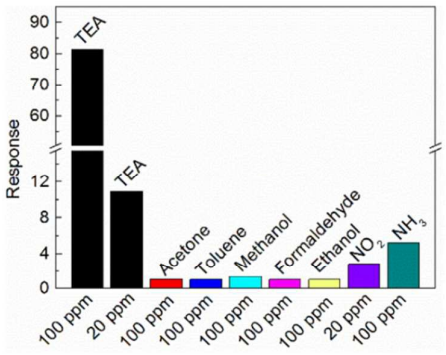

A smart sensor based on PANI-WO_3 nanocomposites loading on PET thin film was fabricated by in situ chemical oxidation polymerization, which not only exhibits high sensitivity and selectivity to triethylamine under room temperature, but also has flexibility, fabricating simplified, economical and wearable characters compared with the recently existing in literatures.